Acta Neuropathologica (2022) 144:1103–1116
https://doi.org/10.1007/s00401-022-02472-x

ORIGINAL PAPER

Regional distribution and maturation of tau pathology among phenotypic variants of Alzheimer's disease

Sanaz Arezoumandan[1,2] · Sharon X. Xie[3] · Katheryn A. Q. Cousins[2] · Dawn J. Mechanic-Hamilton[4,5] · Claire S. Peterson[1,2] · Camille Y. Huang[1] · Daniel T. Ohm[1,2] · Ranjit Ittyerah[6] · Corey T. McMillan[2,5] · David A. Wolk[4,5] · Paul Yushkevich[5,6] · John Q. Trojanowski[5,7] · Edward B. Lee[5,7,8] · Murray Grossman[2] · Jeffrey S. Phillips[2] · David J. Irwin[1,2]

Received: 25 April 2022 / Revised: 2 July 2022 / Accepted: 14 July 2022 / Published online: 23 July 2022

Abstract

Alzheimer's disease neuropathologic change (ADNC) is clinically heterogenous and can present with a classic multidomain amnestic syndrome or focal non-amnestic syndromes. Here, we investigated the distribution and burden of phosphorylated and C-terminally cleaved tau pathologies across hippocampal subfields and cortical regions among phenotypic variants of Alzheimer's disease (AD). In this study, autopsy-confirmed patients with ADNC, were classified into amnestic (aAD, $N=40$) and non-amnestic (naAD, $N=39$) groups based on clinical criteria. We performed digital assessment of tissue sections immunostained for phosphorylated-tau (AT8 detects pretangles and mature tangles), D^{421}-truncated tau (TauC3, a marker for mature tangles and ghost tangles), and E^{391}-truncated tau (MN423, a marker that primarily detects ghost tangles), in hippocampal subfields and three cortical regions. Linear mixed-effect models were used to test regional and group differences while adjusting for demographics. Both groups showed AT8-reactivity across hippocampal subfields that mirrored traditional Braak staging with higher burden of phosphorylated-tau in subregions implicated as affected early in Braak staging. The burden of phosphorylated-tau and TauC3-immunoreactive tau in the hippocampus was largely similar between the aAD and naAD groups. In contrast, the naAD group had lower relative distribution of MN423-reactive tangles in CA1 ($\beta=-0.2$, SE = 0.09, $p=0.001$) and CA2 ($\beta=-0.25$, SE = 0.09, $p=0.005$) compared to the aAD. While the two groups had similar levels of phosphorylated-tau pathology in cortical regions, there was higher burden of TauC3 reactivity in sup/mid temporal cortex ($\beta=0.16$, SE = 0.07, $p=0.02$) and MN423 reactivity in all cortical regions ($\beta=0.4$–0.43, SE = 0.09, $p<0.001$) in the naAD compared to aAD. In conclusion, AD clinical variants may have a signature distribution of overall phosphorylated-tau pathology within the hippocampus reflecting traditional Braak staging; however, non-amnestic AD has greater relative mature tangle pathology in the neocortex compared to patients with clinical amnestic AD, where the hippocampus had greatest relative burden of C-terminally cleaved tau reactivity. Thus, varying neuronal susceptibility to tau-mediated neurodegeneration may influence the clinical expression of ADNC.

Keywords Alzheimer's disease · Neurofibrillary tangles · Tau · Non-amnestic AD

✉ David J. Irwin
dirwin@pennmedicine.upenn.edu

1 Digital Neuropathology Laboratory, Department of Neurology, Perelman School of Medicine, Philadelphia, PA 19104, USA

2 Penn Frontotemporal Degeneration Center, Perelman School of Medicine, Philadelphia, PA 19104, USA

3 Department of Biostatistics, Epidemiology, and Informatics, Perelman School of Medicine, University of Pennsylvania, Philadelphia, PA 19104, USA

4 Department of Neurology, Penn Memory Center, Perelman School of Medicine, Philadelphia, PA 19104, USA

5 Department of Neurology, Penn Alzheimer's Disease Research Center, Perelman School of Medicine, Philadelphia, PA 19104, USA

6 Penn Image Computing and Science Lab, Department of Radiology, Perelman School of Medicine, Philadelphia, PA 19104, USA

7 Center for Neurodegenerative Disease Research, Department of Pathology and Laboratory Medicine, Perelman School of Medicine, Philadelphia, PA 19104, USA

8 Translational Neuropathology Research Laboratory, Department of Pathology and Laboratory Medicine, Perelman School of Medicine, University of Pennsylvania, Philadelphia, PA 19104, USA

Introduction

AD neuropathological change (ADNC) consists of beta-amyloid plaques and neurofibrillary tangles composed of the microtubule-binding protein tau [23]. Cognitive decline and disease severity are strongly correlated with burden of tau pathology in amnestic Alzheimer's disease (AD) [38]; however, ADNC is clinically heterogeneous, and predominant language, visuospatial, behavioral and dysexecutive presentations are not uncommon [2]. Indeed, it is increasingly recognized that ADNC is not an uncommon neuropathological substrate for non-amnestic syndromes in the clinical spectrum of frontotemporal dementia, such as primary progressive aphasia (PPA) [34], behavioral-variant frontotemporal dementia (bvFTD), and corticobasal syndrome (CBS)[29]. Additionally, posterior cortical atrophy (PCA), a "visual variant" [13], and a proposed dysexecutive form of ADNC [53] constitute other non-amnestic presentations of ADNC.

ADNC is also pathologically heterogenous; Murray et al. reported a subgroup of pathologically-defined ADNC patients with sparing of tau pathology in the hippocampus relative to neocortical regions, and many of these neuropathologically-classified patients had distinct non-amnestic clinical features and antemortem imaging findings [37, 55]. Moreover, a recent autopsy study using clinically-defined groups found that non-amnestic cases had more prominent cortical tau pathology compared to typical amnestic AD that related to domain-specific cognitive impairment [43]. The previous histopathological studies focused largely on a subset of mature tangles recognized by thioflavin-S. However, examination of different conformational tau epitopes that track with various stages of tangle progression including neurodegeneration from extracellular ghost pathology, are lacking. With the advent of autopsy-confirmed molecular imaging sensitive to ADNC tau pathology in vivo [14] there is increasing data from living patients suggesting clinically-defined non-amnestic AD syndromes have prominent focal cortical tau pathology that progresses in a manner distinct from amnestic AD [13, 41, 44, 45]. Autopsy studies are rare in these patients, and PET imaging lacks resolution to interrogate hippocampal subfield connectivity that is well-defined in the context of traditional Braak staging of AD tau pathology [8]. Thus, detailed analysis of hippocampal subfield distributions of tau in non-amnestic AD is lacking. Additionally, the specific forms of tau pathology detected by current PET tracers is not entirely clear [35], thus, detailed postmortem work in non-amnestic AD is needed to fully interrogate microscopic anatomy of the hippocampus for various forms of tau pathology in the full spectrum of tangle progression. Traditional histopathological staging is not feasible in non-amnestic AD due to the difficulties in identifying pre-symptomatic autopsies with mild disease; however, tau maturation from pre-tangles and threads to well-formed mature tangles and eventual neuronal death and extrusion of extracellular "ghost tangles" [48] has been well-studied in amnestic AD and suggests earlier implicated regions in AD Braak staging have a greater relative burden of mature NFTs [17]. Moreover, conformation-specific tau antibodies, including TauC3 and MN423, which mark the C-terminal truncation epitopes respectively at aspartate 421 (D^{421}) [15] and glutamate 391 (E^{391}) [40], preferentially label mature tangles and ghost tangles and can provide additional insights into tau progression in the human brain. However, tangle progression in clinical variants of AD is understudied.

Here, we address these gaps in a unique investigation of the regional distribution of tau and maturation of NFT within the well-established anatomic framework of tau spread in hippocampal subfields in non-amnestic AD compared to amnestic AD. We then compare maturation of tau pathology in neocortical regions between amnestic and non-amnestic AD. Our findings reveal distinct regional distributions of mature forms of tau marked by TauC3 and MN423 in clinical variants of ADNC that are suggestive of distinct regional vulnerability and likely temporal progression of regional spread among AD clinical phenotypes.

Materials and methods

Participants

Patients were evaluated at the Penn Frontotemporal Degeneration Center (FTDC) or Alzheimer's Disease Research Center (ADRC) and followed to autopsy at the Penn Center for Neurodegenerative Disease Research (CNDR) as part of ongoing and previous clinical research programs. Patients included in the study were selected from Penn Integrated Neurodegenerative Disease Database (INDD) and had autopsy-confirmed primary diagnosis of ADNC. Patients were classified as non-amnestic (naAD) based on clinical criteria for non-amnestic syndromes designated prospectively using review of standardized clinical assessments at weekly diagnostic consensus meetings at the FTDC or ADRC, including PPA variants [21], bvFTD [46], PCA [11], and CBS [3]. In legacy autopsy samples clinically evaluated prior to modern criteria a retrospective chart review was performed by experienced investigators (SA, KC, JP, DJI) to confirm non-amnestic presentation and clinical phenotype. A similar cohort of patients with amnestic AD (aAD) were selected who met clinical criteria for AD [33] with primary neuropathological diagnosis of ADNC and did not meet exclusion criteria below.

Cases with clinically relevant pathological comorbidities of transitional/limbic or diffuse/neocortical Lewy bodies, hippocampal sclerosis, cerebrovascular disease, or previous structural brain disease were excluded from the cohort, along with those with damaged or missing hippocampal tissue. Mild levels of age-related alpha-synuclein and/or TDP-43 pathology in limbic regions (i.e., brainstem-only or amygdala-only stage Lewy body [30], limbic-predominant age-related TDP-43 encephalopathy) [39] were included. Clinical demographics, mini-mental state examination (MMSE) score closest to death, neuropathological diagnosis data, and ApoE status were obtained from INDD. Our final cohort is summarized in (Table 1).

Neuropathological assessment

At the time of autopsy, fresh brain tissue was sampled and uniformly fixed overnight in neutral buffered formalin. Tissue was processed as previously described [25] and embedded in paraffin for the preparation of 6 µm sections for diagnostic evaluation at CNDR as previously reported [52] according to published criteria [23]. All procedures were performed in accordance with the University of Pennsylvania institutional review board.

Digital neuropathological assessment

Regions stained and analyzed for this study included the hippocampus, which was sampled at the level of the lateral geniculate nucleus, along with cortical regions: superior/middle temporal cortex (SMTC), and middle frontal cortex (MFC), and angular gyrus (ANG). In 45 cases, regions were sampled from the left hemisphere (aAD:20, bvFTD:4, CBS:5, PCA:2, PPA:14), right hemisphere was sampled in 30 cases (aAD:17, bvFTD:5, CBS:3, PPA:5) and this data was not available in 4 cases (aAD:3, CBS:1). In a subset of cases without available neutral buffered formalin fixed tissue (< 6% of sections), we used tissue fixed overnight in 10% ethanol with 150 mm NaCL, as we have previously validated for digital assessment [25]. Tissue sections were prepared from ribbons of 10–15 sections with 6 µm thickness from each paraffin block containing a single cortical region in one setting. Tissue sections were selected from this series of serial sections and immunostained for phosphorylated-tau (AT8), D^{421}-truncated tau (TauC3, monoclonal, Dr Nicholas

Table 1 Demographic and pathological characteristics. The mean and standard deviation reported for age at death, age of onset, and disease duration

	Amnestic AD ($N=40$)	Non-amnestic AD ($N=39$)	p
Sex [Male]	19	20	
Age at death	76.2(8.9)	69.8(10)	0.003
Age of onset[a]	65.6(8.3)	60.7(9.6)	0.02
Disease duration[a]	10.6(4.4)	9.5(4.1)	0.2
Neuropathological diagnosis	ADNC:40	ADNC:39	
Amyloid-β plaque score	A3:40	A2:1 A3:38	
Braak stage	B2:1 B3:39	B3:39	
CERAD neuritic plaque score	C2:1 C3:38	C2:2 C3:37	
Limbic TDP-43 co-pathology	15(37.5%)	7(18%)	0.09
Lewy Body Disease	Amygdala predominant:20(50%) Brainstem predominant:3(7.5%)	Amygdala predominant:12(31%)	0.03
Phenotypic variants[b]	Probable AD:39 Possible AD:1	PPA:19[4] bvFTD:9[3] CBS:9[2] PCA:2[1]	
MMSE score[c]	9.8(7.6)	9.3(7.6)	0.8
APOE genetic status	E2/E3:1 E3/E3:10 E3/E4:16 E4/E4:13	E3/E3: 23 E3/E4:13 E4/E4: 3	

[a]Age of onset was not available for one case in the non-amnestic group

[b]Numbers in the brackets represent number of patients that fulfilled the diagnostic criteria in each clinical subgroup

[c]MMSE score was missing for 1 case in the amnestic and 9 cases in the non-amnestic group

Kanaan, 1:20,000, antigen retrieval with 88% formic acid for 5 min) and E^{391}-truncated tau (MN423, monoclonal, Dr M Novak, 1:250,000, antigen retrieval with 88% formic acid for 5 min) in the Penn Digital Neuropathology lab as described [26].

Immunostained sections were imaged on a digital slide scanner (Aperio AT2, Leica Biosystem, Wetzlar, Germany) in the Penn Digital Neuropathology Lab at 20 × magnification. Images were digitally analyzed using QuPath software (version 0.2.0-m5).

First, hippocampal sections were manually segmented by a trained investigator (SA) into individual subfields in the hematoxylin channel, blinded to density of tau immunoreactivity and clinical group, in the QuPath software using anatomically defined boundaries [1] as described previously [10]. Briefly, hippocampal subfields of interest segmented included dentate gyrus (DG); cornu ammonis (CA) subfields CA4, CA3, CA2, and CA1; subiculum; and entorhinal cortex (ERC) based on the cytoarchitectural features of the layers and anatomical landmarks [12, 24]. The general features used for the segmentations were as follow: DG segmentation represented the granular layer of dentate gyrus. CA4 segmentation was limited to pyramidal cells within the concavity of the DG. CA3 segmentation corresponded to the pyramidal neurons of CA3. CA2 was distinguished from CA3 neurons by higher density of large oval neuronal cells of CA2 pyramidal layer. CA1 subfield was confined to scattered triangular pyramidal cells. For the subiculum, the segmentation started where the stratum radiatum layer of CA1 dissipates and ended where the dark maculated cluster of neurons of the pre-subiculum merge and form a layer (pro-subiculum and subiculum proper). The ERC segmentation consisted of entorhinal cortex, identified by the presence of large island of neurons of layer II, the lamina dissecans of layer IV, and the diagonally oriented cortex of the transentorhinal area (due to the specificity of this cytoarchitectural definition of ERC, we had 40% of cases with available ERC segmentation). Individual subfields which were obscured by significant ripped or damaged tissues, precluding accurate manual segmentation, were excluded from analysis. Figure 1a depicts an AT8 stained hippocampal section of a case with ADNC pathology and representative segmentations of the ROIs investigated in this study. Cortical regions were sampled using a modified belt-transect unbiased method to select representative cortex, as described [25]. The belt-transect method is a reliable procedure for neuropathologic sampling of cortical regions of human brain [4]. In this method the parallel oriented cortex from the sulcal wall is selected for sampling to avoid bias from segmenting areas of the tissue where cortical layers are over or under-represented. This is imperative to reduce bias in digital measurements due to the laminar distribution of tau pathology in AD [42]. Here, a modified belt transect method was used for sampling cortical regions, whereby a trained investigator (SA) used the line tool in QuPath to manually generate two semi-parallel lines to define grey-white matter and pia matter-CSF boundaries

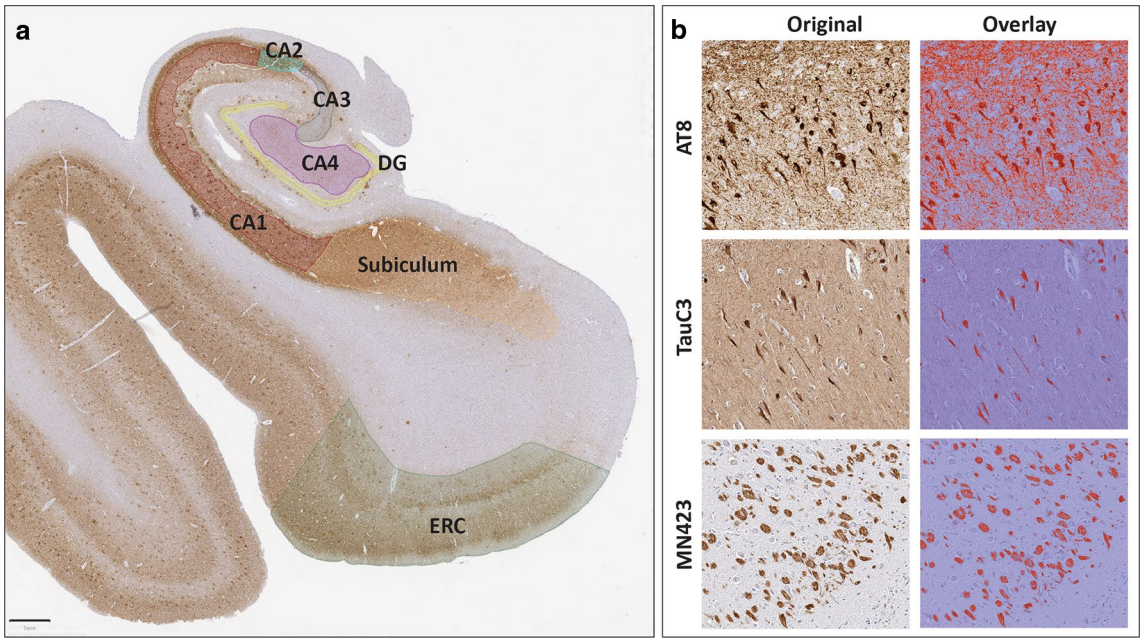

Fig. 1 Hippocampal subfields segmentation and digital histology detection overlay, **a** Segmentation of hippocampal subregions of an AD case stained with AT8; DG: yellow, CA4: pink, CA3: black, CA2: blue, CA1: red, Subiculum: orange, ERC: green. **b** Original image and digital histology detection overlay shown in CA1 region for AT8, TauC3, and MN423; red: positive, purple: negative

of the longest parallel oriented cortex in each section. Next, a script in QuPath creates semi-perpendicular lines in intervals of 250 µm to join the user generated lines to measure the width between these two lines. The program then defines the lateral vertical limits of the ROI at each end where the width of grey matter increases by 0.2 mm. To further reduce bias, we use the create tiles tool to generate 175 µm tiles (Online Resource 1, Supplementary Fig. 1a) in this ROI and a custom script randomly selects a subset of 30% of the tiles for analysis. The final grey matter %AO measurement from each slide image is derived from the average %AO measurement from each random tile per cortical section. In an attempt to further validate our sampling method in this study, we performed alternative sampling using manual segmentation of grey matter with a manual belt-transect method without random tiling and found reliable correlations between the measurements from the two sampling methods (Online Resource 1, Supplementary Fig. 1b, c) and were able to recapitulate our main findings of the study (Online Resource 1, Supplementary Fig. 1d, e).

Next, we used the QuPath program pixel classifier tool with empirically derived positive pixel classifiers for each immunostaining batch of sections as previously validated [19] to calculate the percentage of DAB-positive pixels (%AO) for tau immunoreactivity in each subfield of each image (Fig. 1b). The detailed information and parameters used for positive pixel classifiers and RGB optical density (OD) values for each staining run is provided in Online Resource 1, Supplementary Table 1. Staining batches were performed largely by region and included samples from both clinical groups to reduce batch effects in our main outcomes comparing aAD and naAD groups. For each staining batch, stain RGB OD values were derived empirically from the average value from random tau-positive pathology across five randomly selected images. Stain RGB OD values were used for detecting DAB stain and thresholding based on the minimum OD of positive stain to differentiate pathology signal from background noise. Next, the positive pixel detection algorithms were created for each staining batch based on stain RGB values. An example of digital overlay of positive pixel detection for each staining run is depicted Online Resource 1, Supplementary Fig. 2.

Statistical analysis

Demographic variables were compared between groups using parametric *t*-tests and chi-square tests. We used a square root transformation for %AO values to reduce the skewness of data. We used linear mixed effect models for each antibody (AT8, TauC3, MN423) with square root %AO (sqrt %AO) of tau pathology as the dependent variable and region as an independent variable while adjusting for sex, age at death, disease duration, presence of limbic TDP-43 co-pathology, presence of Lewy body co-pathology, and APOE ε4 carrier status as our base model for each analysis below. LME models account for missing data for individual subfields, and a random intercept is used to account for repeated measures [28] from the same individual as we have done previously [10, 18].

Using this base model, we first examined tau distribution across hippocampal subfields sampled, where the fixed factor region had strata for each subfield (i.e., DG, CA4, CA3, CA2, CA1, Subiculum, and ERC). DG was selected as the reference category to assess the hippocampal distributions, while the interaction term of *clinical group x region* tested divergent regional distributions of tau pathology between clinical groups of AD (i.e., naAD vs aAD) (Online Resource 1, Supplementary Table 2).

In a separate model we tested regional differences between clinical subgroups of naAD in comparison to aAD (i.e. bvFTD vs aAD, CBS vs aAD, and PPA vs aAD) while adjusting for covariates mentioned above. Cases with a clinical diagnosis of PCA were excluded from our clinical subgroup analysis due to the low number of patients in this group ($N=2$) (Online Resource 1, Supplementary Table 3).

Next, we examined the relative distribution of tau in the neocortex with the fixed factor region stratified by cortical regions sampled (i.e., SMTC, MFC, ANG) and included hippocampus CA1 as the reference region. We included the same demographic covariates as above, and our main outcome was the *clinical group x region* interaction (Online Resource 1, Supplementary Table 4). Similarly, a separate model tested for regional differences between clinical subgroups of naAD in comparison to aAD (i.e., bvFTD vs aAD, CBS vs aAD, and PPA vs aAD) while adjusting for covariates as above (Online Resource 1, Supplementary Table 5).

Finally, to test the relative distribution of tau between groups, we averaged the raw %AO for the 3 cortical regions sampled (i.e. neocortical average %AO) and calculated a ratio of neocortical average %AO/CA1%AO for each marker in each individual patient and used Welch two sample *t*-tests to compare the clinical groups. All statistical analyses were performed using version 4.1.1 R statistical software and two-tailed statistics with a significance level of $p<0.05$.

Results

Demographics and clinical features

Patients in the naAD group presented at younger ages compared to aAD ($p=0.02$). In addition, the aAD group had a significantly older age at death compared to naAD ($p=0.003$), while there was no difference in disease duration between the two groups ($p=0.25$). Two groups had

relatively similar ANDC "ABC" score stages [36]; nearly all patients had Braak stage V or VI (Table 1).

Lewy body co-pathology was seen at a higher rate in the aAD group (57.5%) compared to the naAD (31%) ($p=0.03$). In the aAD group, 37.5% of cases had limbic TDP-43 co-pathology, whereas 18% of patients with naAD showed evidence of TDP-43 proteinopathy at autopsy ($p=0.09$). The distribution of phenotypic variants in pathological groups is also shown in (Table 1). There was similar level of global cognitive impairment closest to death in both aAD and naAD groups ($p=0.82$). The rate of patients with at least one copy of APOE ε4 allele was higher among the aAD patients (72.5%) compared to the naAD group (41%) ($p=0.009$).

Hippocampal distribution of p-tau, D^{421}-truncated tau, and E^{391}-truncated tau pathology

We first investigated the regional distribution of phosphorylated-tau (p-tau) pathology immunolabelled by AT8 in the aAD and naAD groups (Fig. 2). In the total cohort, all subregions showed a higher burden of p-tau in relation to DG ($p<0.001$). Particularly, ERC ($\beta=3.3$, $p<0.001$), subiculum ($\beta=4.3$, $p<0.001$), CA1 ($\beta=4.2$, $p<0.001$), and CA2 ($\beta=4.4$, $p<0.001$) appeared to have high levels of p-tau pathology (Fig. 3a). Interestingly, the regional distribution of p-tau pathology across subfields was strikingly similar between the aAD and naAD groups. The analysis of clinical subgroups of naAD found similar distributions of p-tau compared to aAD across hippocampal subfields ($p>0.07$), with the exception of naAD-bvFTD, which showed greater p-tau in ERC ($\beta=1.6$, $p=0.005$).

Next, we explored the distribution of D^{421}-truncated tau, immunostained by TauC3 in hippocampal subfields that selectively detects mature tangles [22] (Fig. 2). We found higher levels of TauC3-immunoreactive tau in ERC ($\beta=0.25$, $p<0.001$), Subiculum ($\beta=0.16$, $p<0.001$), CA1 ($\beta=0.39$, $p<0.001$), and CA2 ($\beta=0.24$, $p<0.001$) compared to DG. Similar to p-tau, there was no significant difference in hippocampal distribution of D^{421}-truncated tau between the aAD and naAD ($p>0.23$) (Fig. 3b). In addition, our analysis of clinical subgroups found no difference between aAD and clinical subgroups of naAD in burden of TauC3 immunoreactive tau in any of the subfields, except for the CBS group with significantly lower D^{421}-truncated tau in ERC ($\beta=-0.36$, $p=0.024$).

Since the clinical groups had similar patterns of p-tau and D^{421}-truncated tau across hippocampal subfields, we next tested for group differences in MN423 reactivity (Fig. 2), which largely labels late "ghost pathology" from tau-mediated neurodegeneration. Overall, MN423-positive ghost tangles were abundant in CA1, presubiculum and ERC. In ERC, MN423-positive ghost tangles were seen frequently in layer II. In the total cohort, MN423-immunopositive pathology was enriched in earlier Braak-stage regions, including ERC ($\beta=0.7$, $p<0.001$), subiculum ($\beta=0.28$, $p<0.001$), CA1 ($\beta=0.65$, $p<0.001$), and CA2 ($\beta=0.49$, $p<0.001$). CA4 also showed a greater burden of ghost tangles in relation to DG ($\beta=0.2$, $p=0.001$), although it was lower in severity than the regions above. Moreover, longer disease duration ($\beta=0.03$, $p=0.001$) was associated with greater overall MN423 immunoreactive tau pathology in the total AD group.

The comparison between the aAD and naAD indicated a lower burden of MN423 reactivity in the naAD group in CA1 ($\beta=-0.29$, $p=0.001$) and CA2 ($\beta=-0.25$, $p=0.005$) (Fig. 3c). Examination of clinical subgroups of naAD indicated a similar pattern of regional sparing of CA1 in bvFTD ($\beta=-0.39$, $p=0.008$), CBS ($\beta=-0.43$, $p=0.005$) and trend level for PPA ($\beta=-0.20$, $p=0.09$) compared to aAD. The bvFTD subgroup had additional relative sparing of MN423 reactivity in CA2 ($\beta=-0.37$, $p=0.012$) compared to the aAD.

Distribution of p-tau, D^{421}-truncated tau, and E^{391}-truncated tau pathology in cortical regions

We examined available cortical tissue to test if naAD had greater relative AT8, TauC3, and MN423 reactivity in the neocortex compared to aAD (Fig. 4).

The interaction term of *clinical group x region* showed no difference in p-tau pathology between the two groups ($p>0.18$) (Fig. 5a), whereas age at death was associated with lower AT8 reactivity in cortical regions compared to CA1 ($\beta=-0.06$, $p<0.001$). Examination of monoclonal antibodies (mAbs) specific for tau C-terminal truncation epitopes that label more mature NFT pathology finds a higher burden of Tau C3 reactivity tau in SMTC in naAD compared to aAD ($\beta=0.16$, $p=0.02$) (Fig. 5b) and greater relative MN423-immunoreactive tau pathology in naAD compared to aAD in all three cortical regions ($\beta=0.4$–0.43, $p<0.001$) (Fig. 5c). Additionally, disease duration ($\beta=0.02$, $p<0.001$) was a significant predictor of relative MN423-positive tau pathology in neocortical regions. Presence of limbic TDP-43 co-pathology was also associated with higher relative MN423 reactivity in cortical regions ($\beta=0.08$, $p=0.047$).

To further test direct comparisons between clinical groups, we calculated the ratio of average tau pathology in neocortical regions to CA1 in each individual patient for each mAb. A higher ratio suggests greater relative neocortical tau burden. The neocortical to CA1 ratio was not significantly different for p-tau pathology labelled by AT8 between aAD and naAD groups ($p=0.64$) (Fig. 6a), while the neocortical to CA1 ratio was significantly higher in the naAD group for both TauC3 ($p=0.047$) (Fig. 6b) and MN423 reactivity ($p=0.007$) (Fig. 6c).

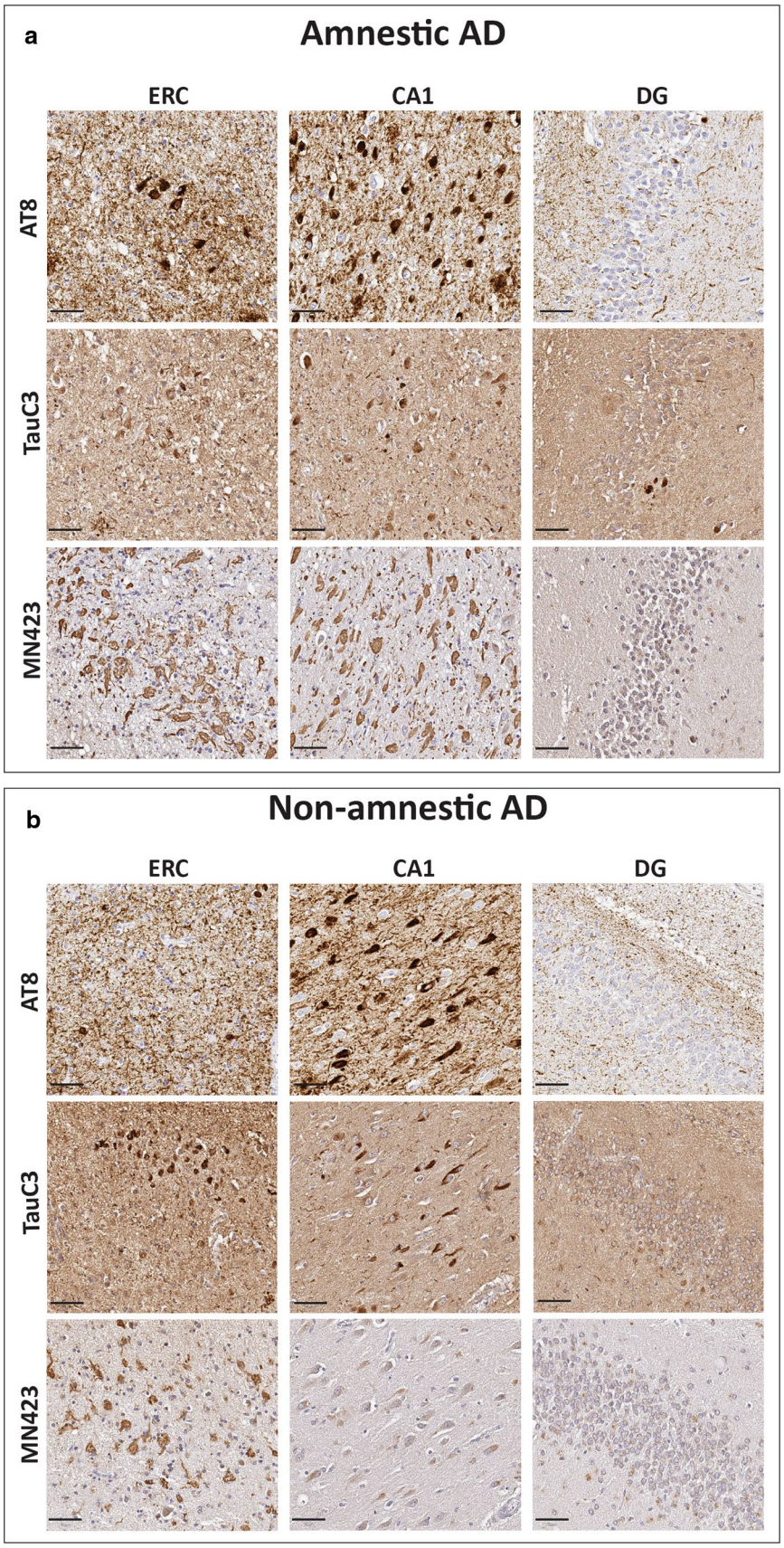

Fig. 2 Tau pathology immunolabelled with AT8, TauC3, and MN423 in hippocampal formation, Representative images of DG, CA1, and layer II of entorhinal region from serial sections immunostained with AT8, TauC3, and MN423 are shown. **a** High levels of AT8-immuopositive p-tau pathology was seen in an aAD case in areas of CA1, and ERC compared to DG that was associated with few tangles and threads detected by TauC3 and high burden of MN423 reactive ghost tangles in CA1 and ERC. **b** A case with naAD with a largely comparable level of p-tau in CA1 region, had few TauC3-reactive tangles in CA1 and ERC and no MN423-immunoreactive ghost tangles in CA1. Scale bar: 50 µm

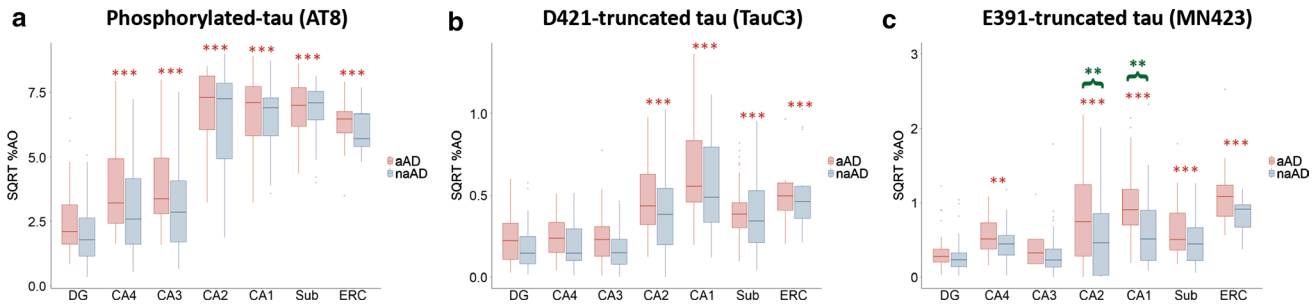

Fig. 3 Hippocampal distribution of phosphorylated-tau, D^{421}-truncated tau, and $E.^{391}$-truncated tau, Boxplots of sqrt %AO with tau pathology in each subfield of hippocampus are shown for markers of AT8, TauC3 and MN423. Red asterisks indicate significant regional differences compared to DG and green asterisks showing the significant *p* values for the interaction term of clinical group x region. (***P*-value < 0.001, **P*-value < 0.01, **P*-value < 0.05)

Finally, we performed subanalyses to account for heterogeneity between the individual naAD clinical subgroups of bvFTD, CBS and PPA. The interaction term of *region x clinical subgroups* suggested similar relative burden of p-tau between bvFTD, CBS, and PPA group and the aAD ($p > 0.13$); whereas we found higher relative TauC3 immunoreactivity in SMTC ($\beta = 0.22$, $p = 0.04$) and MFC ($\beta = 0.33$, $p = 0.003$) in the bvFTD group compared to aAD. TauC3 reactivity was also higher in SMTC region in the PPA group in comparison to the aAD ($\beta = 0.18$, $p = 0.03$). Moreover, we found consistently higher relative neocortical MN423 reactivity across regions in bvFTD, CBS, and PPA groups compared to aAD ($\beta = 0.26$–0.61, $p < 0.017$) (Fig. 7). To address the effect of laterality on our findings, we performed additional statistical analysis while adjusting to the variable of hemisphere and observed similar finding of higher relative cortical MN423 reactivity in all non-amnestic phenotypes compared to aAD (Online Resource 1, Supplementary Table 6).

In our two patients with clinical PCA, we found higher AT8 (×1.7) and MN423 (×6.7) reactivity in ANG compared to SMTC for case#1 and the case#2 showed slightly higher AT8 positive tau in ANG gyrus (×1.63) relative to SMCT, while MN423 reactivity in ANG (×0.8) was largely comparable to SMTC (Online Resource 1, Supplementary Table 7).

Discussion

In this study we investigated the regional distribution and maturation of tau pathology across phenotypic variants of AD using digital measures of phosphorylated and C-terminally truncated tau pathology. Overall, our data suggest that clinical variants of AD appeared to have a similar signature of p-tau burden labelled by AT8 that mirrored traditional Braak staging in the hippocampus; however we found a stepwise increase in relative neocortical reactivity in the naAD group compared to aAD for C-terminally truncated tau markers, TauC3 and MN423, which label increasingly more mature NFT pathology [22, 35]. Indeed, we found a double dissociation, where the aAD had greater relative MN423 reactivity in hippocampal CA1 and CA2 regions compared to patients with naAD, while the naAD had greater relative mature tau pathology identified by both TauC3 and MN423 in cortical regions compared to aAD. These findings suggest non-amnestic AD may have distinct regional vulnerabilities to neurodegeneration and possibly a distinct temporal sequence of tau deposition across limbic and cortical regions.

Hyperphosphorylation of tau at S202/T205 detected by AT8 is considered an early event in NFT formation [20] and generally marks both pretangles and mature tangles in early stages of neurofibrillary change [7]. According to Braak neuropathological staging of AD, NFT changes start in transentorhinal cortex and later appear in the hippocampal formation, in areas of CA1 and subiculum in stages II–IV [8]. Thus, our digital measurements largely recapitulated traditional Braak staging of NFT progression through hippocampal subfields with observed high levels of p-tau pathology in ERC, subiculum, and CA1 of hippocampus. We also found a high burden of p-tau in CA2, where Braak and Braak originally reported interindividual variability in NFT change [8]. We found no difference in hippocampal or neocortical p-tau %AO between clinically-defined groups of aAD and naAD. While these patterns of overall p-tau pathology were similar between clinical AD groups we found more robust differences examining reactivity for mAbs that mark more mature conformers of tau.

TauC3 is a mAb that recognizes caspase cleaved tau at aspartate 421. Caspase activation is one of the mechanisms that induce apoptosis in neurons and is associated with β-amyloid pathology in AD [15]. TauC3-imunoreactive tau is known to identify more mature NFTs in the temporal sequence of NFT maturation [6]. TauC3 recognizes a spectrum of early to mature NFTs including well-formed intracellular tangles that react to amyloid-binding dyes and

a subset of extracellular ghost tangles [31]. Here, consistent with our finding for p-tau, burden of D^{421}-truncated tau was higher in early affected hippocampal subregions of CA1, subiculum and ERC for both clinical groups. Additionally, relative burden of hippocampal TauC3 immunoreactivity was comparable between aAD and naAD, while analysis of cortical regions showed greater relative TauC3 immunoreactive tau in naAD, particularly for the superior/middle temporal cortex. Apoptosis is considered one of the mechanisms leading to neuronal loss in AD [50], given that tau cleavage at D^{421} is an evidence of caspase activation and neuronal death in AD [6], our findings with this marker give insight into possible mechanisms of neuronal vulnerability to tau pathology. We further examined for possible differences in neuronal vulnerability to tau pathology by studying another tau conformational marker that largely labels ghost pathology left behind degenerated tangle-bearing neurons.

While clinical groups of ADNC had a similar overall distribution of p-tau and D^{421}-truncated tau in hippocampus, examination of a E^{391}-truncated tau marker found greater relative mature MN423-reactive pathology in early regions (i.e., CA1) in aAD compared to naAD. Studies in typical amnestic AD support this framework of tangle progression with a greater burden of MN423 in earlier regions such as ERC and CA1 [16]. Truncation at glutamic acid 391, a late cleavage event hypothesized in the progression of NFT maturity, is enriched for mature tangles in addition to extracellular "ghost tangles" from degenerated neurons [27]. Since quantitative measurement of neurodegeneration is challenging in histopathologic studies, the burden of extracellular ghost tangles as reflected by MN423 reactivity could be used as a valuable indicator of neurodegeneration in AD.

Similar to our findings with AT8 and TauC3, the overall hippocampal distribution of MN423 in AD largely corresponded to patterns of tau propagation initially proposed by Braak and Braak [8]; we found high MN423 positive pathology in CA1, subiculum and ERC. Interestingly, CA4 was also an area of high MN423 reactivity, and ghost tangles have been described in nonpyramidal cells of CA4 in Braak stage VI cases [8]. Since the majority of our patients had high level ADNC, it is likely that high MN423 reactivity in CA2 and CA4 compared to DG in our study is suggestive of high Braak stage of our samples.

Importantly, direct comparison of aAD and naAD groups found a higher burden of MN423-immunoreactive tau in all cortical regions for naAD patients compared to aAD, while aAD had greater relative hippocampal MN423-reactivity (Fig. 6c). These data suggest distinct regional patterns of neuronal vulnerability to tau pathology may influence the clinical expression of ADNC. Indeed, our clinical subgroup analysis also found some regional differences between different naAD syndromes. Higher relative cortical D^{421}-truncated tau in MFC and less severely in SMTC in bvFTD compared to aAD, supports previous studies that have explored regional patterns of NFT in non-amnestic AD [43]. Additionally, relative burden of D^{421}-truncated tau was greater in SMTC in PPA group in comparison to aAD, which was in line with previous postmortem [43] and neuroimaging studies [13, 47] including a tau PET study that have described greater tau accumulation in sup/mid temporal cortex in PPA compared to amnestic AD [44]. The asymmetry of pathology has been established in PPA phenotype [34]. Here, majority of the samples ($N=14$) for the PPA group ($N=19$) was collected from the left hemisphere and additional analyses accounting for hemisphere found similar results. Future work can comprehensively compare lateralization of tau conformational marker reactivity in naAD.

Due to small number of cases with PCA phenotype, we could not perform statistical modeling in this group, however inspection of the raw %AO values suggests possible greater relative tau-mediated neurodegeneration in the posterior parietal lobe. Future work in larger number of cases with more expanded sampling of visual association cortex will further clarify regional vulnerability to tau-mediated neurodegeneration in PCA.

Our findings largely align with previous work which focused on reactivity to the amyloid-binding dye, thioflavin S for detection of NFT pathology in ADNC [37, 43]. Importantly, through the use of selective tau conformational antibodies we add novel insights into the cellular processes of tau-mediated neurodegeneration and how these relate to clinical syndromes.

One interpretation of these main findings is that clinical variants of AD have similar cellular patterns of overall tau propagation, as evidenced by p-tau reactivity data (Fig. 6a) but diverge in the specific neuronal populations vulnerable to tau-mediated neurodegeneration, resulting in the greater relative neocortical TauC3 and MN423 reactivity we observed in naAD (Fig. 6b, c). Alternatively, since MN423 data mirrors, in part, the order of temporal progression of tau pathology in AD, the observed discrepancy between aAD and naAD may also suggest a different temporal progression of tau pathology in these AD groups, consistent with the hypothesis that NFT pathology may initiate in neocortical regions in non-amnestic cases and thus may deviate from the overall traditional Braak staging scheme of tau spread in AD.

Indeed, emerging tau PET imaging studies in AD support a potential origin of tau pathology within the neocortex for various non-amnestic phenotypes [41, 44, 45]. These potential interpretations of the data are not mutually exclusive, and there are likely complex biological processes that are difficult to model with postmortem human tissue alone, which provide only limited view at end stage of disease, where onset and rate of progression are difficult to model definitively. Moreover, various conformations of tau

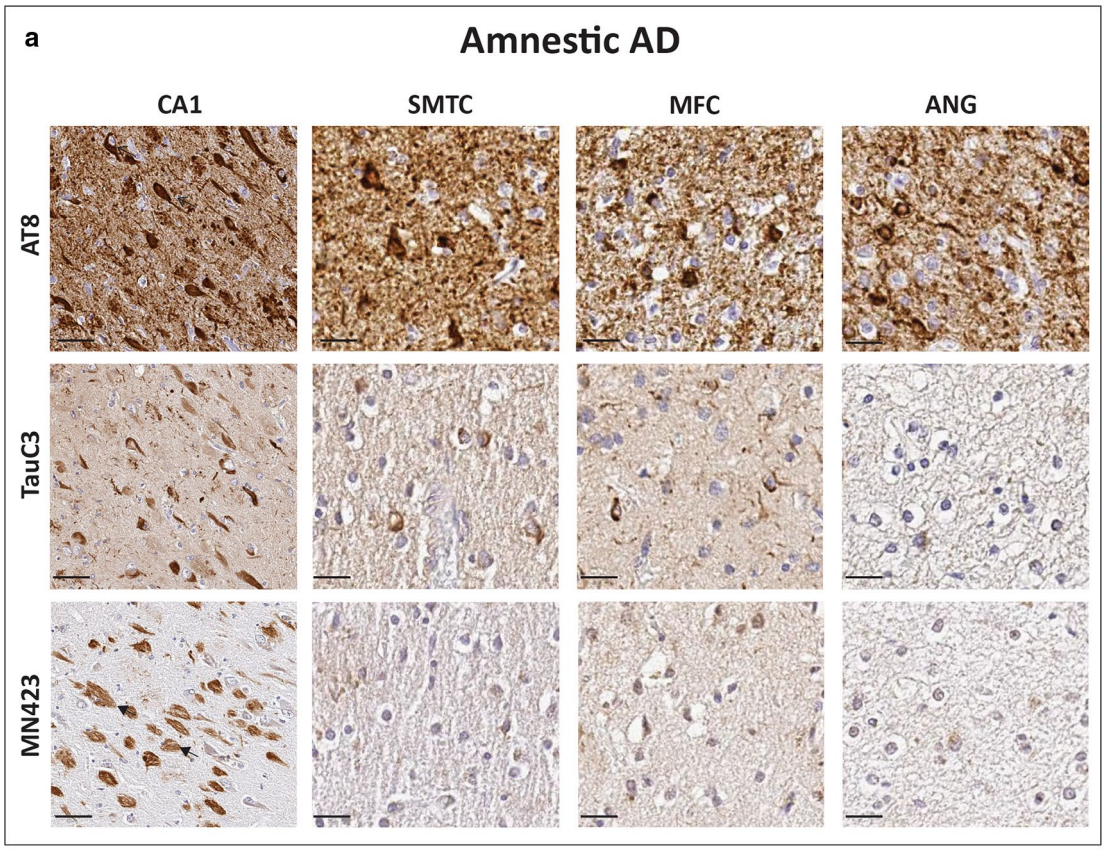
a
Amnestic AD
CA1
SMTC
MFC
ANG
AT8
TauC3
MN423

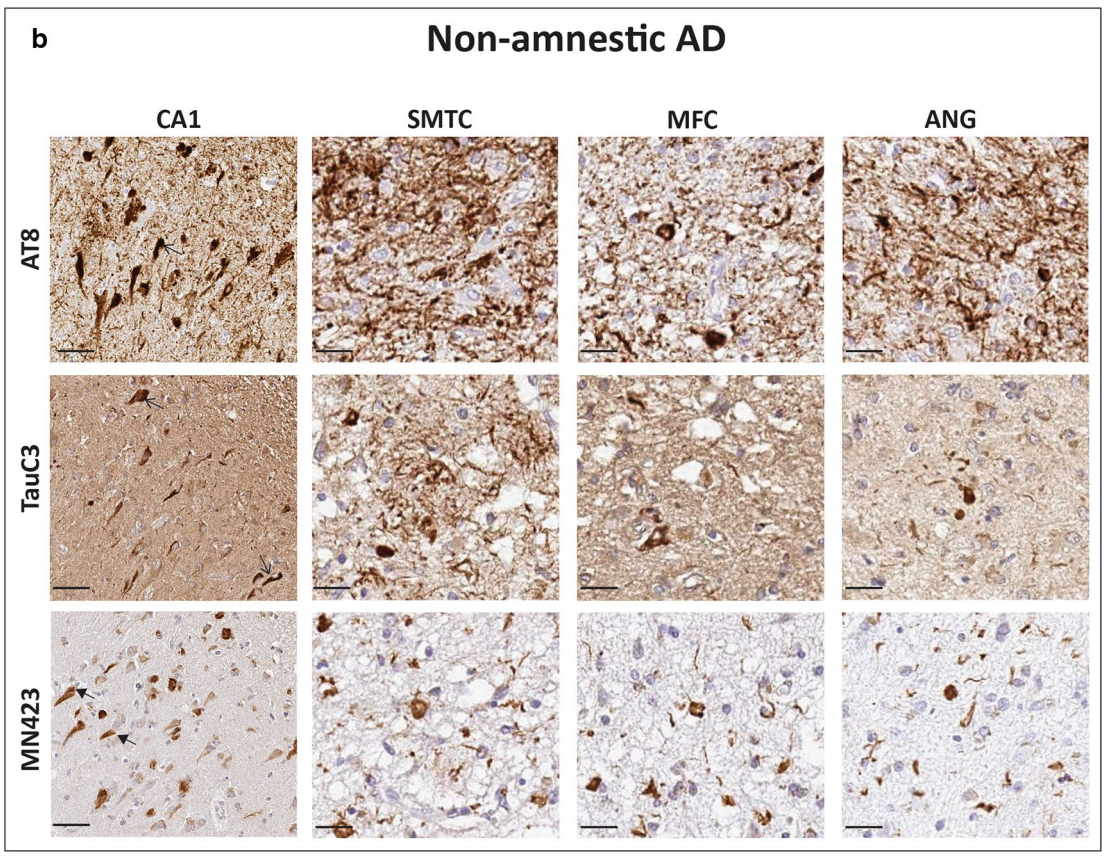
b
Non-amnestic AD
CA1
SMTC
MFC
ANG
AT8
TauC3
MN423

◂**Fig. 4** Tau pathology immunolabelled with AT8, TauC3, and MN423 in neocortical regions and CA1. Representative images of CA1 and layer II/III of neocortical regions of sup/mid temporal cortex (SMTC), middle frontal cortex (MFC), and angular gyrus (ANG) from adjacent sections immunostained with AT8, TauC3, and MN423 are shown. **a** P-tau pathology was seen abundantly in CA1 and cortical regions in a case with aAD. While the adjacent section of CA1 is abundant in TauC3 reactive mature tangles and MN423 reactive ghost tangles, the neocortical regions showed few TauC3 reactive mature tangles and were spared from MN423-immunoreactive ghost tangles. **b** Neocortical areas and CA1 subfield immunostained for AT8 showed high levels of p-tau pathology in a case with naAD, few TauC3 immunoreactive tangles in CA1, MFC, and ANG while SMTC region showed high TauC3 reactivity. MN423 immunoreactive ghost tangles seen abundantly in cortical regions and few extracellular ghost tangles in CA1. Open arrow: mature tangle, closed arrow: ghost tangle. Scale bar in CA1 images: 50 µm, Scale bar in cortical images: 20 µm

pathology currently cannot be differentiated in vivo and detected with sufficient resolution with molecular imaging techniques such as tau-PET to measure spatiotemporal changes in microscopic structures such as the perforant pathway to elucidate these mechanisms. Therefore, studying various conformations of tau in postmortem histopathologic studies is of direct future relevance for understanding cellular processes involved in posttranslational modification of tau, cellular vulnerability, and tau-mediated neurodegeneration in AD. Thus, future work incorporating antemortem imaging data and possibly human-derived cell culture models or other patient-derived biological readouts with postmortem validation can clarify these issues.

We carefully accounted for other variables that could influence the severity of tau pathology in our samples. Common co-pathologies with ADNC, including TDP-43 proteinopathy and Lewy bodies, are known to influence the clinical heterogeneity and cognitive function in AD [49]. Interestingly, similar to a recent report [32] we found that limbic TDP-43 co-pathology did not clearly influence AT8 or TauC3 reactivity in AD, but we did find a novel association of limbic TDP-43 with higher MN423 immunoreactivity in cortical regions. This finding could indicate that biological processes of tau-mediated neurodegeneration may be linked to the development of TDP-43 co-pathology in ADNC. Future studies are needed to determine the role of TDP-43 and other co-pathologies on acceleration of tau maturation and clinical presentation of AD. Similar to previous reports, our naAD group was younger and had a lower frequency of APOE ε4 compared to aAD group [54]. Interestingly increased disease duration was linked to higher overall MN423-reactivity. This suggests there is increased

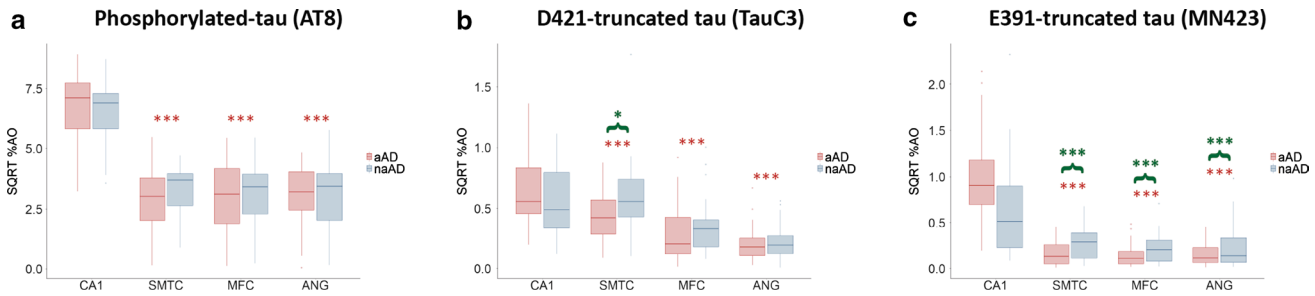

Fig. 5 AT8, TauC3, and MN423-immunoreactive tau pathology in neocortical region, Boxplots of sqrt %AO with phosphorylated-tau, D^{421}-truncated, and E^{391}-truncated tau in CA1 and cortical regions of middle frontal cortex (MFC), sup/mid temporal cortex (SMTC) and angular gyrus (ANG). Red asterisks indicate significant regional differences in comparison to CA1 and green asterisks showing the significant *p* values for interaction term of clinical group x region. (***P*-value < 0.001, **P*-value < 0.01, **P*-value < 0.05)

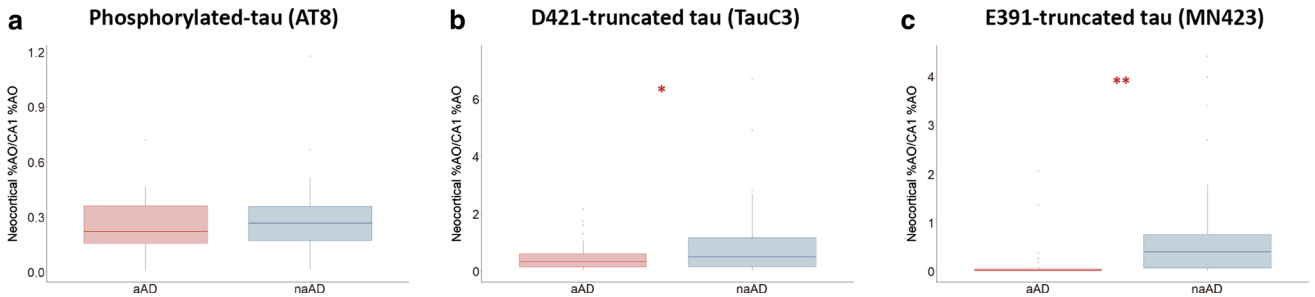

Fig. 6 Ratio of neocortical-%AO to CA1-%AO for AT8, TauC3, and MN423 immunoreactive tau, Boxplots of averaged neocortical to CA1 ratio of %AO with phosphorylated-tau, D^{421}-truncated tau, and E^{391}-truncated tau shown for the aAD and naAD groups. Red asterisks showing the significant levels for *t*-tests. (***P*-value < 0.01, **P*-value < 0.05)

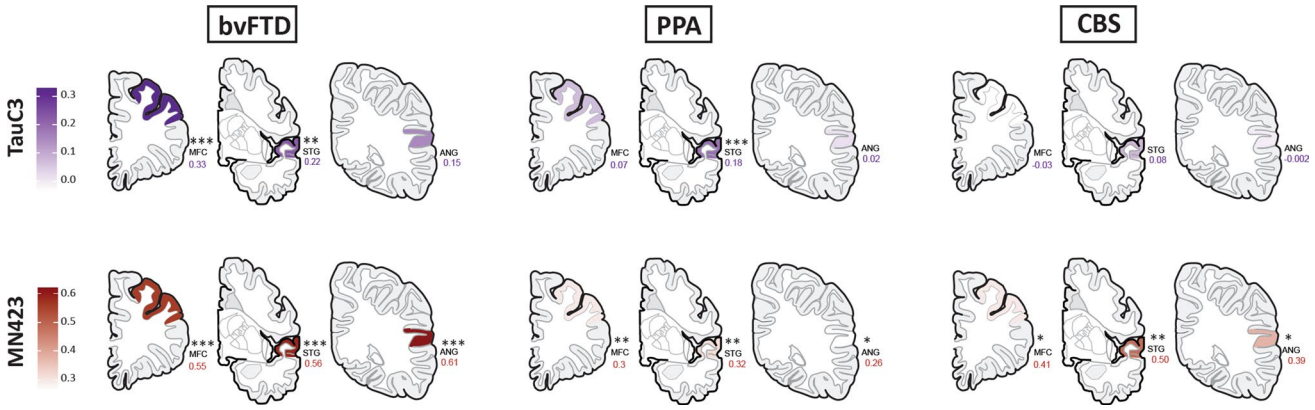

Fig. 7 Regional heatmaps for C-terminally truncated tau pathologies in non-amnestic phenotypes, Heatmaps represent beta weights for burden of neocortical tau relative to CA1 in different clinical phenotypes, in comparison to aAD. Beta weights were extracted from LME models for analysis of clinical subgroups (Online Resource 1, Supplementary Table 5)

accumulation MN423-reactive tau pathology with longer survival, consistent with the association of this tau conformation with late-stage NFTs. Previously, one study reported that higher prevalence of the APOE ε 4 allele is linked to elevated TauC3 and MN423-positive NFT in hippocampus when compared to controls [5]. Our findings suggested no association between APOE ε4 carrier status and burden of AT8 or MN423 immunoreactive tau ($p > 0.5$). This discrepancy may be due in part to differences in study design, as our focus was on comparison of clinical variants of AD with largely similar high-level "ABC" profiles (Table 1). Importantly, regional differences in MN423-reactivity between aAD and naAD groups remained robust even after accounting for these covariates.

The validated digital analysis approach used in this study gave us the ability to analyze images and generate data for > 800 slides, including immunostaining with different makers of tau conformations in multiple regions for 79 patients. Future studies with larger cohorts with more extensive cortical sampling can be conducted with these methods, and this high dimensional dataset of gold-standard human brain histopathology can be analyzed with computational methods [9] to further model disease propagation.

It is important to consider the limitations in the anatomical interrogation of the perforant pathway and cortical regions in our relatively limited pathological sampling from 6 um thick sections; however, we were conservative in our manual segmentations using established methods [1] and a validated digital image analysis approach [25] for the large-scale autopsy cohort presented here. Moreover, we were limited in examining more detailed cortical regional pathology comparatively in clinical subgroups of naAD due to the relatively small sample size of these rare clinical variants of AD. Indeed, further large-scale studies in larger cohorts with more detailed histopathological sampling, such as those facilitated by ex vivo MRI [51], are needed to fully examine patterns of tau maturation in the context of cortical connectivity to model tau propagation in non-amnestic AD. Finally, our cohort is referred from tertiary academic center and may not fully reflect heterogeneity of AD in the community [49].

These limitations notwithstanding, our unique analysis of tau maturation markers in naAD suggests distinct biological profiles of vulnerability to tau-mediated neurodegeneration. Possible divergent neuronal populations vulnerable to tau-mediated neuropathology and temporal sequence of tau spread in the human brain may contribute to the clinical heterogeneity of ADNC. These data will inform emerging biomarker studies of naAD and mechanistic work on neuronal vulnerability to tauopathies.

Supplementary Information The online version contains supplementary material available at https://doi.org/10.1007/s00401-022-02472-x.

Acknowledgements We would like to thank Theresa Schuck and John Robinson for their assistance in autopsy coordination. We thank Dr. M Novak for the generous gift of MN423 antibody. We are grateful to Dr. Nicholas Kanaan for the gift of TauC3 antibody. We extend gratitude to the patients and families whose effort for participation in research and brain donation make this work possible. Finally, we would like to acknowledge Dr. John Q. Trojanowski (1946-2022) who has had an enormous and lasting impact on the field of AD and related disorders. This work was supported by NIH grants NINDS R01- NS109260-01A1, NIA P01-AG066597, NIA P30-AG072979 (formerly P30-AG10124), NIA R01-AG054519-02, Penn Institute on Aging, Brightfocus Foundation #A2016244S, Alzheimer's Association (AARF-D-619473, AARF-D-619473-RAPID) and the Wyncote Foundation.

References

1. Adler DH, Wisse LEM, Ittyerah R et al (2018) Characterizing the human hippocampus in aging and Alzheimer's disease using a

computational atlas derived from ex vivo MRI and histology. Proc Natl Acad Sci U S A 115:4252–4257. https://doi.org/10.1073/pnas.1801093115
2. Alladi S, Xuereb J, Bak T et al (2007) Focal cortical presentations of Alzheimer's disease. Brain J Neurol 130:2636–2645. https://doi.org/10.1093/brain/awm213
3. Armstrong MJ, Litvan I, Lang AE et al (2013) Criteria for the diagnosis of corticobasal degeneration. Neurology 80:496–503. https://doi.org/10.1212/WNL.0b013e31827f0fd1
4. Armstrong RA (2003) Quantifying the pathology of neurodegenerative disorders: quantitative measurements, sampling strategies and data analysis. Histopathology 42:521–529. https://doi.org/10.1046/j.1365-2559.2003.01601.x
5. Basurto-Islas G, Luna-Muñoz J, Guillozet-Bongaarts AL et al (2008) Accumulation of aspartic acid421- and glutamic acid391-cleaved tau in neurofibrillary tangles correlates with progression in Alzheimer disease. J Neuropathol Exp Neurol 67:470–483. https://doi.org/10.1097/NEN.0b013e31817275c7
6. Binder LI, Guillozet-Bongaarts AL, Garcia-Sierra F, Berry RW (2005) Tau, tangles, and Alzheimer's disease. Biochim Biophys Acta BBA - Mol Basis Dis 1739:216–223. https://doi.org/10.1016/j.bbadis.2004.08.014
7. Braak E, Braak H, Mandelkow EM (1994) A sequence of cytoskeleton changes related to the formation of neurofibrillary tangles and neuropil threads. Acta Neuropathol (Berl) 87:554–567. https://doi.org/10.1007/BF00293315
8. Braak H, Braak E (1991) Neuropathological stageing of Alzheimer-related changes. Acta Neuropathol (Berl) 82:239–259. https://doi.org/10.1007/BF00308809
9. Chen M, Ohm DT, Phillips JS et al (2022) Divergent histopathological networks of frontotemporal degeneration proteinopathy subytpes. J Neurosci Off J Soc Neurosci 42:3868–3877. https://doi.org/10.1523/JNEUROSCI.2061-21.2022
10. Coughlin DG, Grossman M, Trojanowski JQ, Irwin DJ (2021) Hippocampal subfield pathologic Burden in Lewy body diseases versus Alzheimer's disease. Neuropathol Appl Neurobiol. https://doi.org/10.1111/nan.12698
11. Crutch SJ, Schott JM, Rabinovici GD et al (2017) Consensus classification of posterior cortical atrophy. Alzheimers Dement J Alzheimers Assoc 13:870–884. https://doi.org/10.1016/j.jalz.2017.01.014
12. Duvernoy HM, Cattin F, Risold P-Y (2013) The human hippocampus: functional anatomy, vascularization and serial sections with MRI, 4. Aufl. https://doi.org/10.1007/978-3-642-33603-4
13. Firth NC, Primativo S, Marinescu R-V et al (2019) Longitudinal neuroanatomical and cognitive progression of posterior cortical atrophy. Brain 142:2082–2095. https://doi.org/10.1093/brain/awz136
14. Fleisher AS, Pontecorvo MJ, Devous MD et al (2020) Positron emission tomography imaging with [18F] flortaucipir and postmortem assessment of Alzheimer disease neuropathologic changes. JAMA Neurol 77:829–839. https://doi.org/10.1001/jamaneurol.2020.0528
15. Gamblin TC, Chen F, Zambrano A et al (2003) Caspase cleavage of tau: linking amyloid and neurofibrillary tangles in Alzheimer's disease. Proc Natl Acad Sci U S A 100:10032–10037. https://doi.org/10.1073/pnas.1630428100
16. Garcıa-Sierra F, Wischik CM, Harrington CR et al (2001) Accumulation of C-terminally truncated tau protein associated with vulnerability of the perforant pathway in early stages of neurofibrillary pathology in Alzheimer's disease. J Chem Neuroanat 22:65–77. https://doi.org/10.1016/S0891-0618(01)00096-5
17. Ghoshal N, Garcıa-Sierra F, Wuu J et al (2002) Tau conformational changes correspond to impairments of episodic memory in mild cognitive impairment and Alzheimer's disease. Exp Neurol 177:475–493. https://doi.org/10.1006/exnr.2002.8014
18. Giannini LAA, Xie SX, McMillan CT et al (2019) Divergent patterns of TDP-43 and tau pathologies in primary progressive aphasia. Ann Neurol 85:630–643. https://doi.org/10.1002/ana.25465
19. Giannini LAA, Xie SX, Peterson C et al (2019) Empiric methods to account for pre-analytical variability in digital histopathology in frontotemporal lobar degeneration. Front Neurosci 13:682. https://doi.org/10.3389/fnins.2019.00682
20. Goedert M, Jakes R, Vanmechelen E (1995) Monoclonal antibody AT8 recognises tau protein phosphorylated at both serine 202 and threonine 205. Neurosci Lett 189:167–170. https://doi.org/10.1016/0304-3940(95)11484-E
21. Gorno-Tempini ML, Hillis AE, Weintraub S et al (2011) Classification of primary progressive aphasia and its variants. Neurology 76:1006–1014. https://doi.org/10.1212/WNL.0b013e31821103e6
22. Guillozet-Bongaarts AL, Garcia-Sierra F, Reynolds MR et al (2005) Tau truncation during neurofibrillary tangle evolution in Alzheimer's disease. Neurobiol Aging 26:1015–1022. https://doi.org/10.1016/j.neurobiolaging.2004.09.019
23. Hyman BT, Phelps CH, Beach TG et al (2012) National Institute on aging–Alzheimer's association guidelines for the neuropathologic assessment of Alzheimer's disease. Alzheimers Dement J Alzheimers Assoc 8:1–13. https://doi.org/10.1016/j.jalz.2011.10.007
24. Insausti R, Amaral DG (2012) Hippocampal Formation In: Human Nervous System. Elsevier, Amsterdam, pp 896–942
25. Irwin DJ, Byrne MD, McMillan CT et al (2016) Semi-automated digital image analysis of pick's disease and TDP-43 Proteinopathy. J Histochem Cytochem Off J Histochem Soc 64:54–66. https://doi.org/10.1369/0022155415614303
26. Irwin DJ, Cohen TJ, Grossman M et al (2012) Acetylated tau, a novel pathological signature in Alzheimer's disease and other tauopathies. Brain J Neurol 135:807–818. https://doi.org/10.1093/brain/aws013
27. Khuebachova M, Verzillo V, Skrabana R et al (2002) Mapping the C terminal epitope of the Alzheimer's disease specific antibody MN423. J Immunol Methods 262:205–215. https://doi.org/10.1016/S0022-1759(02)00006-6
28. Laird NM, Ware JH (1982) Random-effects models for longitudinal data. Biometrics 38:963–974. https://doi.org/10.2307/2529876
29. Lee SE, Rabinovici GD, Mayo MC et al (2011) Clinicopathological correlations in corticobasal degeneration. Ann Neurol 70:327–340. https://doi.org/10.1002/ana.22424
30. Leverenz JB, Hamilton R, Tsuang DW et al (2008) RESEARCH ARTICLE: empiric refinement of the pathologic assessment of lewy-related pathology in the dementia patient. Brain Pathol 18:220–224. https://doi.org/10.1111/j.1750-3639.2007.00117.x
31. Luna-Muñoz J, Peralta-Ramirez J, Chávez-Macías L et al (2008) Thiazin red as a neuropathological tool for the rapid diagnosis of Alzheimer's disease in tissue imprints. Acta Neuropathol (Berl) 116:507–515. https://doi.org/10.1007/s00401-008-0431-x
32. McAleese KE, Walker L, Erskine D et al (2020) Concomitant LATE-NC in Alzheimer's disease is not associated with increased tau or amyloid-β pathological burden. Neuropathol Appl Neurobiol 46:722–734. https://doi.org/10.1111/nan.12664
33. McKhann GM, Knopman DS, Chertkow H et al (2011) The diagnosis of dementia due to Alzheimer's disease: recommendations from the national institute on aging-Alzheimer's association workgroups on diagnostic guidelines for Alzheimer's disease. Alzheimers Dement J Alzheimers Assoc 7:263–269. https://doi.org/10.1016/j.jalz.2011.03.005
34. Mesulam M-M, Weintraub S, Rogalski EJ et al (2014) Asymmetry and heterogeneity of Alzheimer's and frontotemporal pathology

in primary progressive aphasia. Brain J Neurol 137:1176–1192. https://doi.org/10.1093/brain/awu024
35. Moloney CM, Lowe VJ, Murray ME (2021) Visualization of neurofibrillary tangle maturity in Alzheimer's disease: a clinicopathologic perspective for biomarker research. Alzheimers Dement J Alzheimers Assoc 17:1554–1574. https://doi.org/10.1002/alz.12321
36. Montine TJ, Phelps CH, Beach TG et al (2012) National institute on aging-Alzheimer's association guidelines for the neuropathologic assessment of Alzheimer's disease: a practical approach. Acta Neuropathol (Berl) 123:1–11. https://doi.org/10.1007/s00401-011-0910-3
37. Murray ME, Graff-Radford NR, Ross OA et al (2011) Neuropathologically defined subtypes of Alzheimer's disease with distinct clinical characteristics: a retrospective study. Lancet Neurol 10:785–796. https://doi.org/10.1016/S1474-4422(11)70156-9
38. Nelson PT, Alafuzoff I, Bigio EH et al (2012) Correlation of Alzheimer disease neuropathologic changes with cognitive status: a review of the literature. J Neuropathol Exp Neurol 71:362–381. https://doi.org/10.1097/NEN.0b013e31825018f7
39. Nelson PT, Dickson DW, Trojanowski JQ et al (2019) Limbic-predominant age-related TDP-43 encephalopathy (LATE): consensus working group report. Brain 142:1503–1527. https://doi.org/10.1093/brain/awz099
40. Novak M, Jakes R, Edwards PC et al (1991) Difference between the tau protein of Alzheimer paired helical filament core and normal tau revealed by epitope analysis of monoclonal antibodies 423 and 7.51. Proc Natl Acad Sci U S A 88:5837–5841
41. Ossenkoppele R, Schonhaut DR, Schöll M et al (2016) Tau PET patterns mirror clinical and neuroanatomical variability in Alzheimer's disease. Brain J Neurol 139:1551–1567. https://doi.org/10.1093/brain/aww027
42. Pearson RC, Esiri MM, Hiorns RW et al (1985) Anatomical correlates of the distribution of the pathological changes in the neocortex in Alzheimer disease. Proc Natl Acad Sci U S A 82:4531–4534
43. Petersen C, Nolan AL, de Paula França Resende E et al (2019) Alzheimer's disease clinical variants show distinct regional patterns of neurofibrillary tangle accumulation. Acta Neuropathol (Berl) 138:597–612. https://doi.org/10.1007/s00401-019-02036-6
44. Phillips JS, Das SR, McMillan CT et al (2018) Tau PET imaging predicts cognition in atypical variants of Alzheimer's disease. Hum Brain Mapp 39:691–708. https://doi.org/10.1002/hbm.23874
45. Phillips JS, Nitchie FJ, Da Re F et al (2021) Rates of longitudinal change in 18 F-flortaucipir PET vary by brain region, cognitive impairment, and age in atypical Alzheimer's disease. Alzheimers Dement J Alzheimers Assoc. https://doi.org/10.1002/alz.12456
46. Rascovsky K, Hodges JR, Knopman D et al (2011) Sensitivity of revised diagnostic criteria for the behavioural variant of frontotemporal dementia. Brain J Neurol 134:2456–2477. https://doi.org/10.1093/brain/awr179
47. Quantitative neurofibrillary tangle density and brain volumetric MRI analyses in Alzheimer's disease presenting as logopenic progressive aphasia | Elsevier Enhanced Reader. https://doi.org/10.1016/j.bandl.2013.02.003
48. Schmidt ML, Gur RE, Gur RC, Trojanowski JQ (1988) Intraneuronal and extracellular neurofibrillary tangles exhibit mutually exclusive cytoskeletal antigens. Ann Neurol 23:184–189. https://doi.org/10.1002/ana.410230212
49. Schneider JA, Arvanitakis Z, Bang W, Bennett DA (2007) Mixed brain pathologies account for most dementia cases in community-dwelling older persons. Neurology 69:2197–2204. https://doi.org/10.1212/01.wnl.0000271090.28148.24
50. Smale G, Nichols NR, Brady DR et al (1995) Evidence for apoptotic cell death in Alzheimer's disease. Exp Neurol 133:225–230. https://doi.org/10.1006/exnr.1995.1025
51. Tisdall MD, Ohm DT, Lobrovich R et al (2022) Ex vivo MRI and histopathology detect novel iron-rich cortical inflammation in frontotemporal lobar degeneration with tau versus TDP-43 pathology. NeuroImage Clin 33:102913. https://doi.org/10.1016/j.nicl.2021.102913
52. Toledo JB, Van Deerlin VM, Lee EB et al (2014) A platform for discovery: the university of pennsylvania integrated neurodegenerative disease biobank. Alzheimers Dement J Alzheimers Assoc 10:477-484.e1. https://doi.org/10.1016/j.jalz.2013.06.003
53. Townley RA, Graff-Radford J, Mantyh WG et al (2020) Progressive dysexecutive syndrome due to Alzheimer's disease: a description of 55 cases and comparison to other phenotypes. Brain Commun. https://doi.org/10.1093/braincomms/fcaa068
54. van der Flier WM, Pijnenburg YA, Fox NC, Scheltens P (2011) Early-onset versus late-onset Alzheimer's disease: the case of the missing APOE ε4 allele. Lancet Neurol 10:280–288. https://doi.org/10.1016/S1474-4422(10)70306-9
55. Whitwell JL, Dickson DW, Murray ME et al (2012) Neuroimaging correlates of pathologically defined subtypes of Alzheimer's disease: a case-control study. Lancet Neurol 11:868–877. https://doi.org/10.1016/S1474-4422(12)70200-4